Design of D-Shaped Sensor Based on Surface Plasmon Resonance in Photonic Crystal Fiber

M. Mercy Anitha [1] , N. Aravindan [2], A. Sivanantha Raja [3]
[1] PG Student
[2]Teaching Research Assistant
[3]Associate professor
Department of Electronic and Communication Engineering
Alagappa Chettiar Government College of Engineering & Technology, Karaikudi, 630003

***Abstract*:- A recognizing characteristics of refractive index (RI) and temperature sensor design based on a D- shaped photonic crystal fiber (PCF). The D-shaped flat surface is layered with a silver film to construct surface plasmon resonance (SPR) for the RI sensing, while a single hole in the solid (PCF) is filled with benzene to form a directional resonance coupling for the temperature sensing. With a strong coupling between the core mode and the resonance modes, the maximum sensitivities of the RI and the temperature are as high as 1900 nm/RIU and 5.49 nm/ K .Since surface plasmon resonance designs are used to avoid the need of metal coating in the fiber holes and use high RI sensing medium for temperature sensing.**

Key words : photonic crystal fiber sensor , surface plasmon resonance ,directional coupling ,dual-parameter

INTRODUCTION

surface plasmon resonance (SPR)sensor, also called optical sensors based on excitation of surface plasmons can be excite at certain wavelengths, The sensing principle is an optical phenomenon in which a TMpolarized light beam satisfies the resonance condition (phase and energy match)and excites the free electron density longitudinal oscillation at the metal/dielectric interface SPR act as the thin film refractometer that can detect small changes in the refractive index(RI)occurring at the surface of a metal film (e.g. ,silver or gold) . It is fundamental principle behind many colour-based biosensor [1]. Among this PCF based design have two mechanism directional resonant coupling and surface plasmon resonance (SPR), Typical sensor based on directional resonant coupling has been proposed where only one of the holes surrounding the fiber core is filled with analyte [2]. However, in practical operation, these PCFs will be difficult to be coated with the metal films and filled with the analytes because the size of the fiber hole is as small as several microns. Most important, if the analyte change during the measurement period, emptying and re-filling of the fibre is required these disadvantages can be overcome by using D-shaped or exposed-core PCFs [3]. In these ways, the metal and analyte can be directly deposited on the expose section of these PCFs, thus it can simplify the sensor fabrication and benefit the analyte changing.

The designed a fiber optical temperature sensor based on SPR with silver as the metallic layer and Benzene as the sensing layer, due to the flexible design of the structure , the PCFs can also provide a new method to achieve phase matching between a core mode and plasmon mode [4].The variations in the RI of the analytes can be detected by following characteristics of transmitted light .In this paper, we design a temperature sensor based on SPRs supported by D-shaped fiber sensor are coated with a silver layer and filled with a large thermo-optic coefficient liquid mixture (benzene and graphene).Temperature variation will induce changes of refractive indices of the liquid mixture, thus leading to the shift of the plasmonic peak that will be recorded. when the resonance condition between a core mode and a plasmon mode of the light propagation in the fiber is satisfied at specific wavelength, the energy of the core mode will transfer to a highly lossy plasmon mode. thus, an obvious peak in the loss spectrum of the core mode will observed at this wavelength region [5]. However, it is important to note that in these temperature sensors, the sensing medium is filled into the cladding holes of the PCF. And to preserve the index-guiding character of the PCF, the sensor was limited to the sensing medium with RI lower than that of the fibre material, typically below 1.42 in the case of the silica fibre [12]– [14]. This makes it difficult to utilize some high RI sensing medium, such as toluene, benzene [15], liquid crystals [16], etc. Furthermore, the metal coating in the fibre holes is also required in these proposed sensors [12]– [14].

DESIGN AND ANALYSIS

The schematic of the D-shaped based on SPR sensor in Fig.1.the lattice pitch is Λ=8μm, the diameters of uniform, For RI sensing operation, the fiber is side-polished to form a flat plane where a 40 nm-thick silver film is coated, and then exposed to the analyte.

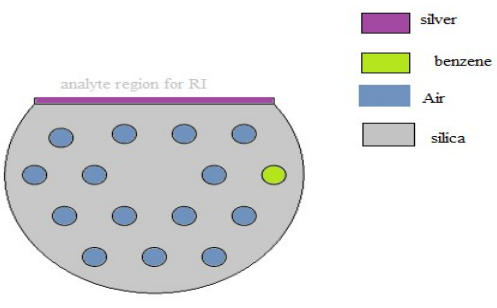

Fig. 1. Schematic of the all-D shaped PCF

The polishing depth from the fiber centre to the polished surface is fixed to h = 1.2Λ. The wavelength dependent RI of the silver is given by the Drude model [6]. Such design can only support a RI-dependent ypolarized resonance peak [7]. For temperature sensing operation, a large thermo-optic coefficient liquid (hexagonal sensing medium) is filled into the only hole of the PCF to form a resonator which can couple with the core mode at resonance wavelength where a temperature-dependent resonance peak will be excited [8], [9]. The electromagnetic modes of the fiber are calculated by using finite element method (FEM). Here, we use the Gaussian-like (HE11-like) modes as the core modes which we will distinguish HE11x (the predominantly xpolarized) mode and HE11y (the predominantly y-polarized) mode

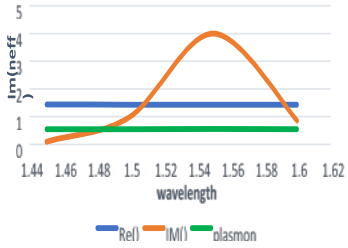

I. Dispersion relations of the y-polarized core mode (HE11y mode) and the plasmon mode

(II) Electric field distributions of the y-polarized

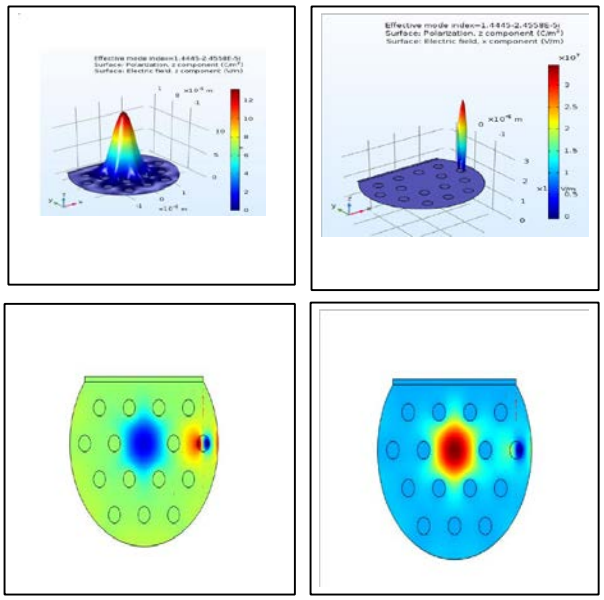

Fig. 2. (I) Dispersion relations of the y-polarized core mode (HE11y mode) and the plasmon mode with na = 1.44 and nt = 1.48. (II) Electric field distributions of the y-polarized (a) core mode at λ = 1.33 μm, (b) plasmon mode at λ = 1.45 μm and (c) core mode at resonance wavelength λ = 1.55 μm. Arrows indicate the polarized direction of the electric field

A. Sensing Principle of SPR

Theoretically, the resonance coupling between core modes and resonance modes can occur if their effective RIs (neff) are equal. The resonance is characterized by an obvious peak of the core mode loss spectrum, which indicates the largest energy transfer between them [6]-[8], [10], [11]. Fig. 2(I) shows the neff of the HE11y modes and the plasmon modes when the RI of the analyte (na) is 1.44 and the RI of the sensing medium (nt) is 1.48.

As the imaginary part of the neff curve [Im(neff)] shown in Fig. 2(I), the resonance peak is located at 1.55 μm [dot (c)] where the real part of the neff [Re(neff)] of the HE11y mode and that of the plasmon mode are equal. The peak is excited at this resonance wavelength due to the energy transfer into the plasmon mode from the core mode. The electric field distributions of the modes in Fig. 2(II) also show the energy transfer between the two modes. At the non-resonance wavelengths, the two modes [Figs. 2(a) and 2(b)] show distinctive patterns respectively. At the resonance wavelength, they become mixed [Fig. 2(c)] which implies that a portion of core mode energy penetrates into the plasmon mode. Thus, an obvious peak in the core mode loss spectrum is observed. When the na is varied, the Re(neff) of the plasmon mode displaces accordingly, thus leading to a shift in the position of the resonance wavelength [dot (c)]. Consequently, the na variation can be detected by measuring the y-polarized resonance peak shift.

B. Sensing Principle of Directional Resonance Coupling

In principle, the resonance coupling between fundamental modes of the fiber core and the liquid-filled waveguide is impossible when the RI of the liquid is higher than that of the background (nbg), because the fundamental mode of high RI liquid-filled waveguide has the neff above the background index (neff > nbg) while the fundamental mode of the PCF central core has neff < nbg. However, the higher-order modes of the liquid-filled waveguide with fields expanding out of the liquid are confined by the air-silica structure, and thus have smaller neff which will be equal (or close) to that of the silica core fundamental mode at a certain wavelength [10], [11]. And the resonance coupling between the two modes can happen near the resonance wavelengths. Here, we use the Gaussian-like (HE11-like) modes as the core modes and thus only consider the coupling mode combinations HE11x-TM1 and HE11y-TE1 [18]. The difference between the resonance wavelengths of the two coupling mode combinations is several nanometres [12]. Therefore, we take the example of the mode combination HE11x-TM1 to illustrate the coupling phenomenon.

The neff curves of the HE11x and the TM1 modes when the na is 1.44 and the nt is 1.48 are presented in Fig. 3.1. It can be seen from Fig. 3(a) that the original two modes will split into another two new modes and interact with each other near the resonance wavelengths (points C and D), forming supermodes. At the shorter wavelength range away from the point C, the energy of the HE11x mode is confined in core area perfectly (Inset A) and transferred to the TM1 mode as wavelength increasing (Inset C). At longer wavelengths, the energy is totally transferred into the TM1 mode (Inset E). For the TM1 mode, the energy transfer is contrary to that for the HE11x mode.

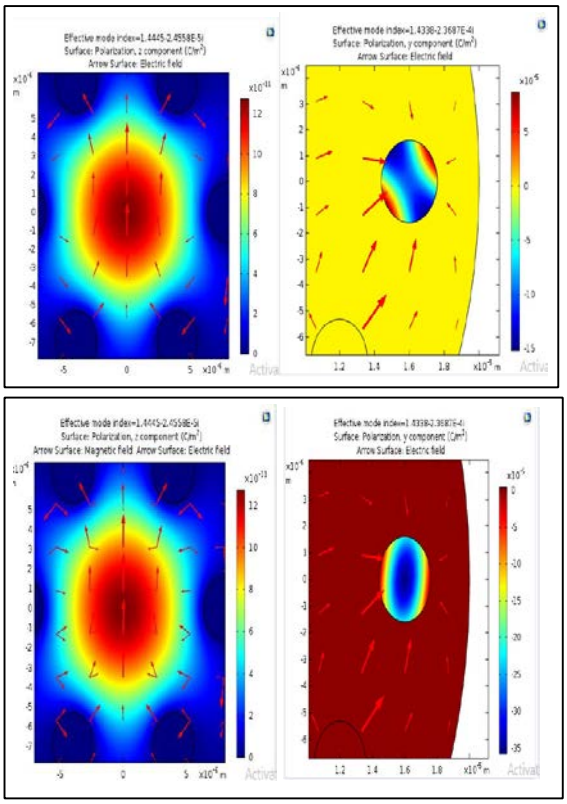

Fig.3 Electric Field distribution of polarized modes (a)HE_{11x} -TM_{01} (b)$HE_{11\,y}$-TE_{01}.

Eventually the energy is thoroughly transferred into the HE11x mode at longer wavelengths. The Im(neff) curves of the two modes in the Fig. 3(b) can also show the energy transfer between the two modes. As the solid curve shown, the mode loss follows the HE11x mode part before the resonance wavelength and switches to the TM1 mode after passing through it. For the dashed curve, the mode loss follows an opposite trend which is from the TM1 mode to the HE11x mode. The energy transfer (coupling) we presented here are also consistent with the phenomenon reported in [13]. As the energy transferring, an obvious peak in the HE11x mode loss spectrum is observed at the resonance wavelength. The temperature variation can cause the nt changing, hence changing the neff of the TM1 node, and resulting in different resonance wavelengths. Thus, it can be detected by tracking the x-polarized peak shift.

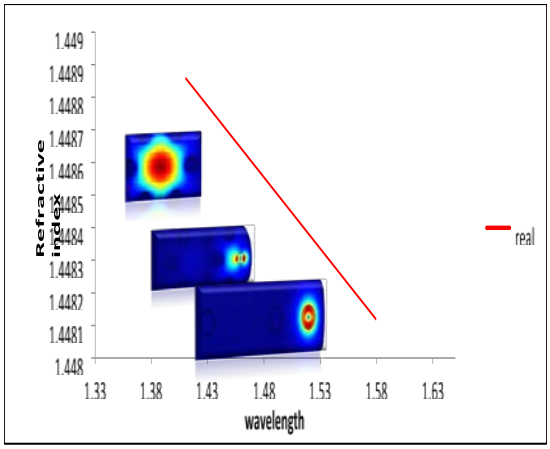

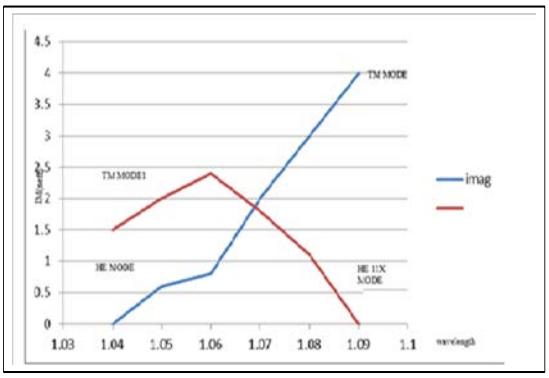

Fig.3.1 Real& Imaginary Part Of Effective Index curves of the mode combination HE11x-TM1 withn_{a} and n_{t}.

III. RESULTS AND DISCUSSION

To demonstrate potential of the proposed sensor for RI and temperature sensing, we present the loss spectra of the core modes in Fig. 4 for the case when the na is slightly varied from and then nt is changed from 1.48. As shown in Fig. 4, the two polarized peaks can shift independently. The y-polarized peak shifts 19 nm when the na is varied from 1.44, and the x-polarized peak shifts 105 nm as the nt changing from 1.48. Therefore, by following the shifts of the y- and x-polarized peaks, the variations of the na and the nt can be detected simultaneously. Note that the other y-polarized peak formed by the mode combination HE11y-TE01 at longer wavelength is not obvious because of the high loss of the core mode. Moreover, it can be eliminated artificially by monitoring the x-polarized peak wavelength because they have the same resonance wavelength.

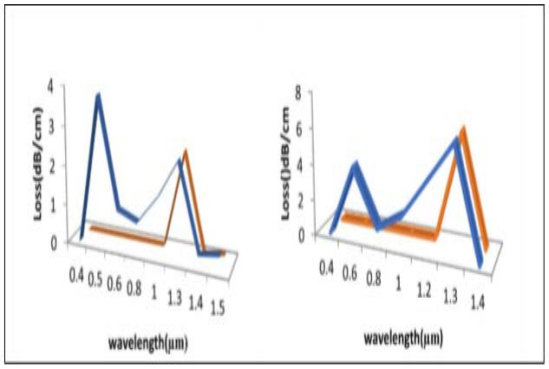

Fig. 4. Loss spectra of the two polarized core modes when (a) na at 1.4489 and nt at 1.4849, (b) na at 1.4486 and nt at 1.4847 (c) na at 1.4484 and nt at 1.4841 (d)na at 1.4481 and nt at 1.4837, (Red line indicated by nt and Blue line indicated by na).

Figure 4. shows the different spectra of a y-polarized core mode when the na changes from 1.44 For reference, losses in decibels per meter are defined as [15]:

$$\alpha_{loss} = 8.686.\ k_0\ \mathrm{Im}[neff](dB/m)$$

here, $k_0 = 2\pi/\lambda$ is the wavenumber with λ being in meters. By variable the refractive index, as in Fig. 4, the neff of the core mode can be readily tuned, thus changing the peak wavelength and sensor sensitivity.

In the case of the RI sensing, the na variations can be detected by measuring the shift of the y-polarized peak (Δλpeak). As shown in Fig. 4, the Δλpeak is 19 nm for the na changing from 1.44(Δna = 0.01), and the corresponding sensitivity in term of RI units (RIU) is 1900 nm/RIU. The wavelengths and the sensitivities of the y-polarized peak with na from 1.44. As a result, the sensitivity increases as na increasing and the maximum sensitivity is 15700 nm/RIU for the na changing from 1.45. This phenomenon is caused by the extension of the evanescent wave in the sensing region. When the na gets closer to the RI of the fiber core material (in this sensor is 1.45), the RI-contrast between the fiber core and the sensing region is reduced, and more energy of evanescent wave will extend into in the sensing region, resulting in more photon interaction and higher sensitivity [14]. However, as the na increasing (typically above 1.42), higher order plasmon modes can also be excited [15], which may introduce noise and make the detection of the na more difficult.

By measuring the transmission spectrum of the sensor fiber, refractive -index resolution of

$$S(nm/RIU) = \frac{\Delta\lambda peak(na)}{\Delta na}$$

In the case of the temperature sensing, Temperature variations will induce changes of the nt, thus leading to different x-polarized loss spectra that will be recorded. We assume the hole is filled with the fluid benzene that possesses the nt = 1.479 at 20 °C, and a thermal coefficient of dn/dT = -7.594×10-4 K-1[15]. The thermal coefficient of the silica are much smaller than that of the fluid, thus the temperature induced changes can be attributed predominantly to changes in the RI of the fluid benzene. The wavelengths and the shifts of the x-polarized peak at different nt are presented. The maximal peak shifts is 105 nm for the nt changing from 1.46 (T =45 °C) to 1.47 (T = 32 °C), and the corresponding temperature sensitivity is 5.49 nm/K. which is higher than that of PCF-based SPR temperature sensors [12]– [14]. by defining temperature sensitivity as [16]

$$s_\lambda[nm/k] = \Delta_\lambda peak/\Delta T$$

Furthermore, the maximal temperature sensitivity and its detection range in this sensor can be adjusted by using some tuneable nt sensing media such as liquid mixture [13] or liquid crystal [15], because the sensor shows higher sensitivity when the nt gets close to the na.

IV. CONCLUSION

In this paper, we present a special sensor design in a D-shaped all-solid PCF to simultaneously realize the RI and temperature detections. Two resonance mechanisms are used in this sensor, which are the SPR for the RI sensing and directional resonance coupling for the temperature sensing. The D-shaped plane coated with a silver film can only support a y-polarized peak when the SPR occurs. The only hole in the PCF filled with fluid benzene can excite an obvious x-polarized peak when the directional resonance coupling happens. By tracking the two polarized peaks shifts, the variations of the RI and temperature can be detected simultaneously. It would be very suitable for detecting temperature-dependent RI of the analyte in chemical, medical and biological areas, and also can be used for monitoring single changes in RI or temperature. By increasing wavelength, the effective mode index of x is decreasing and effective mode index of y also decreasing. By repeating the same for wavelength starting from 1.45 to 1.65 by taking interval of 0.2 [um]and we got some sequence wise decreasing effective index of x and y pol calculate the loss spectra and temperature changed.

REFERENCE

[1] B. Shuai, L. Xia, Y. Zhang, and D. Liu, “A multi-core holey fibre based plasmonic sensor with large detection range and high linearity,” Opt. Exp., vol. 20, no. 6, pp. 5974–5986, Mar. 2012.
[2] E. Klantsataya, A. François, H. Ebendorff -Heidepriem, P. Hoffmann, and T. M. Monro, “Surface plasmon scattering in exposed core optical fiber for enhanced resolution refractive index sensing,” Sensors, vol. 15, no. 10, pp. 25090–25102, Sep. 2015.
[3] N. Luan, R. Wang, W. Lv, and J. Yao, “Surface plasmon resonance sensor based on exposed-core microstructured optical fibres,” Electron. Lett., vol. 51, no. 9, pp. 714–715, Apr. 2015.
[4] N. Luan, R. Wang, W. L v, and J. Yao, “Surface plasmon resonance sensor based on D-shaped microstructured optical fiber with hollow core,” Opt. Exp., vol. 23, no. 7, pp. 8576–8582, Apr. 2015.
[5] Y. Peng, J. Hou, Z. Huang, and Q. Lu, “Temperature sensor based on surface plasmon resonance within selectively coated photonic crystal fiber,” Appl. Opt., vol. 51, no. 26, pp. 6361–6367, Sep. 2012.

[6] [7] N. Luan, R. Wang, Y. Lu, and J. Yao, “Simulation of surface plasmon resonance temperature sensor based on liquid mixture-filling microstructured optical fiber,” Opt. Eng., vol. 53, no. 6, Jun. 2014, Art. ID 067103. [8] N. Luan, C. Ding, and J. Yao, “A refractive index and temperature sensor based on surface plasmon resonance in an exposed-core microstructured optical fiber,” IEEE Photon. J., vol. 8, no. 2, Apr. 2016, Art. ID 4801608. [9] A. Samoc, “Dispersion of refractive properties of solvents: Chloroform, toluene, benzene, and carbon disulfide in ultraviolet, visible, and near-infrared,” J. Appl. Phys., vol. 94, no. 9, pp. 6167–6174, Nov. 2003. [10] J. Li, S. T. Wu, S. Brugioni, R. Meucci, and S. Faetti, “Infrared refractive indices of liquid crystals,” J. Appl. Phys., vol. 97, no. 7, Mar. 2005, Art. ID 073501.

[7] N. Luan, R. Wang, W. Lv, and J. Yao, “Surface plasmon resonance sensor based on D-shaped microstructured optical fiber with hollow core,” Opt. Exp., vol. 23, no. 7, pp. 8576–8582, Apr. 2015.

[8] Y. Peng, J. Hou, Z. Huang, and Q. Lu, “Temperature sensor based on surface plasmon resonance within selectively coated photonic crystal fiber,” Appl. Opt., vol. 51, no. 26, pp. 6361–6367, Sep. 2012.

[9] N. Luan, R. Wang, Y. Lu, and J. Yao, “Simulation of surface plasmon resonance temperature sensor based on liquid mixture-filling microstructured optical fiber,” Opt. Eng., vol. 53, no. 6, Jun. 2014, Art. ID 067103. [14] N. Luan, C. Ding, and J. Yao, “A refractive index and temperature sensor based on surface plasmon resonance in an exposed-core microstructured optical fiber,” IEEE Photon. J., vol. 8, no. 2, Apr. 2016, Art. ID 4801608. [15] A. Samoc, “Dispersion of refractive properties of solvents: Chloroform, toluene, benzene, and carbon disulfide in ultraviolet, visible, and near-infrared,” J. Appl. Phys., vol. 94, no. 9, pp. 6167–6174, Nov. 2003. [16] J. Li, S. T. Wu, S. Brugioni, R. Meucci, and S. Faetti, “Infrared refractive indices of liquid crystals,” J. Appl. Phys., vol. 97, no. 7, Mar. 2005, Art. ID 073501.

[10] D. K. C. Wu, B. T. Kuhlmey, and B. J. Eggleton, “Ultrasensitive photonic crystal fiber refractive index sensor,” Opt. Lett., vol. 34, no. 3, pp. 322–324, Feb. 2009.

[11] D. K. C. Wu, K. J. Lee, V. Pureur, and B. T. Kuhlmey, “Performance of refractive index sensors based on directional couplers in photonic crystal fibers,” J. Lightw. Technol., vol. 31, no. 22, pp. 3500–3510, Nov. 2013. [19] A. D. Rakić, A. B. Djurišić, J. M. Elazar, and M. L. Majewski, “Optical properties of metallic films for vertical-cavity optoelectronic devices,” Appl. Opt., vol. 37, no. 22, pp. 5271–5283, Aug. 1998.